A modular tool for analyzing cascade impactors data to improve exposure assessment to airborne nanomaterials

Sébastien Bau, Olivier Witschger

Journal of Physics: Conference Series **429** (2013) 012002 doi:10.1088/1742-6596/429/1/012002

A modular tool for analyzing cascade impactors data to improve exposure assessment to airborne nanomaterials

Sébastien Bau and Olivier Witschger

Institut National de Recherche et de Sécurité (INRS), Laboratoire de Métrologie des Aérosols, Rue du Morvan, CS 60027, 54519 Vandoeuvre Cedex, France

E-mail: sebastien.bau@inrs.fr

Abstract. Cascade impactors are widely used to provide particle size distributions for the study of aerosols in workplaces and ambient air. In the frame of exposure assessment to airborne particles, one of their main advantages is the possibility to perform further off-line analysis (e.g. electron microscopy, physical-chemical characterization by XRD, ICP-MS, etc.) on the collected samples according to particle size. However, the large channel width makes the particle size distributions not enough size-resolved. Furthermore, in spite of the sharpness of the collection efficiency curves, the existence of an overlap between stages renders data interpretation difficult. This work aim was to develop a modular program allowing the inversion of data stemming from cascade impactors based on the mass (or any quantity) collected on each impaction stage. Through a precise description of the collection efficiency curves of the different stages, the software provides a continuous curve (from 100 to 1000 points) using the Markowski method, and more particularly the Twomey iterative algorithm, according to several publications about inverse problems in cascade impactors. An additional option consists in determining the experimental error at each point of the inverse curve, performed by realizing several consecutive inversions. The inversion procedure was first tested and optimized for the case of the SIOUTAS personal sampler. Validation of the calculation was performed considering theoretical aerosols. Then, the software was used for two sets of data obtained during field measurement campaigns.

1. Introduction

Nanomaterials offer applications in fields as wide-ranging as health, food and agriculture, energy, materials, and transport. In parallel, their unique properties raise also questions about their potential related health effects. Due to their rising use, exposure of people working in research laboratories, staff in state-run or public industry is probably increasing. Consequently, assessing inhalation exposure to airborne nanoparticles constitutes an important challenge [1].

Conventionally, occupational exposure to particulate compounds is characterized by the mass concentration combined with the size range of particles penetrating different regions of the respiratory system (inhalable, thoracic and alveolar fractions, as defined by [2]). This approach to occupational exposure is applied to all chemical substances (except for fibers where the concentration is expressed in terms of number of fibers per unit of air volume) found as aerosols, whatever the particle size. To ensure continuance in occupational exposure assessment and in absence of specific regulation for nanoparticles, it seems necessary to pursue measuring particle mass size distribution in workplace atmospheres.

In addition, there are already several published studies that reveal that exposure (*via* the inhalation route) could be characterized by nano-sized and respirable particles during production and handling of manufactured nanomaterials as well as the use of products that contain manufactured nanomaterials [3, 4]. This is one more reason why, in the few strategies for assessing workplace exposure to airborne nanomaterials already proposed, there are the cascade impactors [5, 6].
Cascade impactors have been studied and modeled extensively; they constitute the instrument of choice for the determination of aerosol mass size distributions [7]. As a consequence, there is a wide variety of cascade impactors commercially available, with various cutoff diameters, flow rates and sampling substrates. Associated to analyses (gravimetric, physical-chemical, etc.) performed on each impaction stage, they provide the mass size distribution of the aerosol averaged over the sampling period.
Presenting the cascade impactor data in a histogram ignores information on particle size distribution within each impactor stage and does not take into account the possible overlap between them, *i.e.* that the particles of a given diameter may deposit over several stages [8].
The objective of this study was to develop and test a generic inversion tool devoted to post-analyzing data from cascade impactor measurements. According to several publications about inverse problems in cascade impactors, the software realizes the data inversion using the Markowski method, and more particularly the Twomey iterative algorithm. The results provide a continuous curve defined by 100 to 1000 data points.
From this inverted curve, several particulate concentrations can be determined, such as those corresponding to:

- The conventional health-related fractions [2] used in the field of occupational health;
- The Particulate Matter fractions (PM_{10}, $PM_{2.5}$, PM_1, and even $PM_{0.1}$) used in the field of ambient air quality (non-occupational);
- The lung-deposited fractions [9] as recently recommended by ISO [10] for better estimation of exposure, especially when submicrometer particles are significant.

Furthermore, these data can be converted into any other metric related to the initial one (*e.g.* from mass to number or surface area concentration) that might be more relevant regarding potential health effects (see *e.g.* [11, 12]).

2. Inversion software

2.1. Mathematical description

Within cascade impactors, particles are separated according to their aerodynamic properties, related to their inertia. The parameter governing impaction is the Stokes number (*Stk*), defined by the ratio of the stopping distance of a particle to a characteristic dimension of the obstacle, corresponding here to the radius of a circular nozzle [13]:

$$Stk(d_p) = \frac{\tau \cdot U}{\frac{d_j}{2}} = \frac{\rho_p \cdot d_p^2 \cdot Cu(d_p) \cdot U}{9 \cdot \eta_g \cdot d_j}$$

where ρ_p is the particle density, Cu the slip correction coefficient, U the particle velocity, η_g the gas viscosity and d_j the nozzle diameter. The Stokes number can be used to predict whether or not a particle will impact ($Stk \gg 1$) or not ($Stk \ll 1$) on an impaction plate.
Although collection efficiency (E) depends on particle size, it is not easily related to the Stokes number [14]. Thus, the actual collection efficiency curves are usually determined experimentally by measuring responses of monodisperse calibration aerosols [15-26]. In this work, the following general expression was used:

$$E(d_p) = \left[1 + \left(\frac{d_{p,50}}{d_p}\right)^{2s}\right]^{-1}$$

where $d_{p,50}$ corresponds to the cutoff diameter and s represents the stiffness of the collection efficiency curve. Their values are specific to an impactor model, and mainly depend on its nominal flow rate and stage geometry. Each stage of a cascade impactor will consequently be described by a set of ($d_{p,50}$, s)-values.

For a cascade impactor made of N stages, the probability to collect a particle of diameter d_p on the i^{th} stage is given by the Kernel function:

$$k_i(d_p) = E_i(d_p) \cdot \prod_{j=i+1}^{N} \left[1 - E_j(d_p)\right] \qquad i = 1, \dots, N$$

The determination of a continuous size distribution of the aerosol sampled, notated $f(x)$, based on the N observations, notated m_i, consists in solving the Fredholm integral equations:

$$m_i = \int_0^{\infty} k_i(x) \cdot f(x) \cdot dx + \epsilon_i\,, \qquad i = 1, \dots, N$$

where ϵ corresponds to the uncertainty associated to the observation for each stage. The last equation constitutes the common start point of all inversion algorithms, commonly used under discrete form:

$$m_i = \sum_{j=1}^{M} k_i(x_j) \cdot f(x_j) \cdot \Delta x_j + \epsilon_i, \qquad i = 1, \dots, N\,; j = 1, \dots, M$$

where M is the number of points where the function f is defined in discrete form.

The latter equation, called Fredholm equation in the remainder of this paper, constitutes the condition to be fulfilled to ensure that the inversion procedure has completed. Indeed, when Fredholm equation is satisfied, the difference between observed (m_i) and calculated quantity for stage i ($\sum_{j=1}^{M} k_i(x_j) \cdot f(x_j) \cdot \Delta x_j$) is less or equal to the tolerated error (ϵ_i).

The aim of the inversion procedure is to determine the values of the aerosol size distribution $f(x_j)$ allowing Fredholm equation to be satisfied on each stage. Because the number of points expected is higher than the number of stages ($M \gg N$), the inversion problem is ill-posed and does not admit a unique solution based on a finite set of observations.

2.2. Short description of the inversion method implemented within the software

A deterministic method mainly based on the work of Twomey [27] was chosen to invert data from cascade impactors. Among its main advantages, this non linear iterative method does not assume a mathematical model for the aerosol size distribution resulting from the inversion procedure.

Initiated by Chahine [28], the algorithm proposed consists in multiplying the function at p^{th} iteration by a weighting factor taking into account the Kernel function:

$$f^{(p+1)}(x_k) = f^{(p)}(x_k) \cdot \prod_{i=1}^{N} \left[1 + \left(R_i^{(p)} - 1\right) \cdot k_i(x_k)\right]$$

with:

$$R_i^{(p)} = \frac{m_i}{\sum_{j=1}^{M} k_i(x_j) \cdot f^{(p)}(x_j) \cdot \Delta x_j}$$

Practically, when the resulting function converges to the solution, then:

$$R_i^{(p)} \to 1 \Longrightarrow f^{(p+1)}(x_k) \to f^{(p)}(x_k)$$

Because the function resulting from Twomey's algorithm is particularly dependent on initial supposition and conserves its roughness, the calculation procedure was improved by smoothing the resulting function $f(x_j)$ [29] and by enlarging the weighting functions to avoid important variations due to the narrowness of cascade impactors Kernel functions [30].
Figure 1 is a schematic of the resolution algorithm.

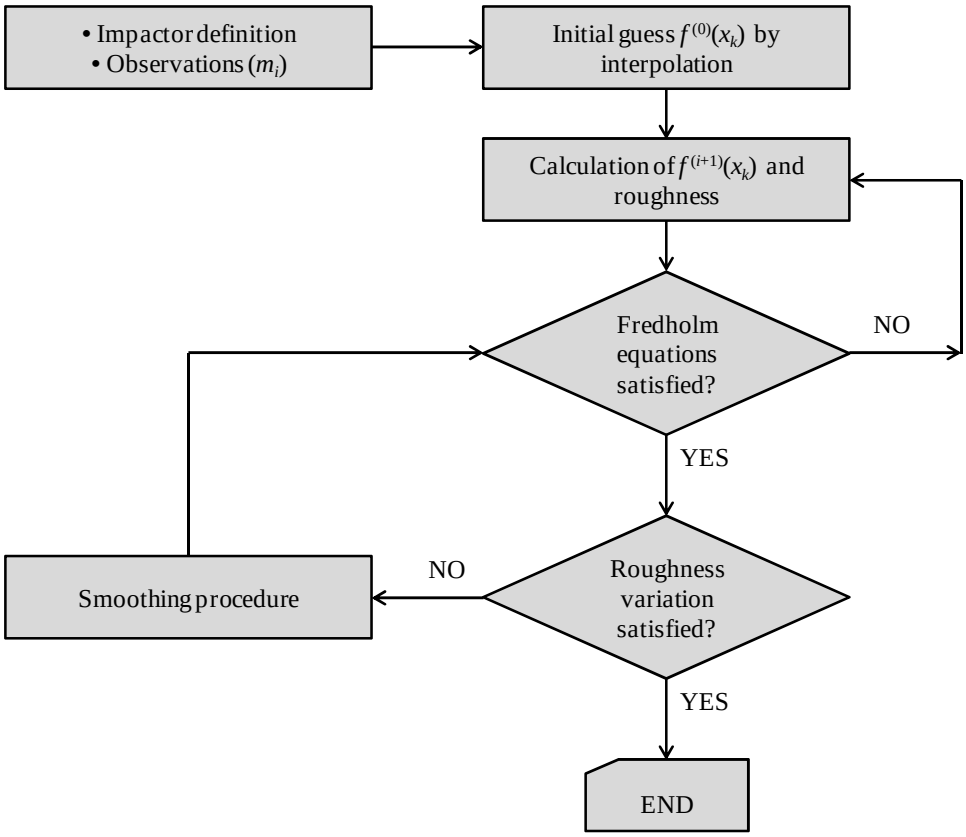

Figure 1. General resolution scheme implemented within the inversion software.

2.3. Software features
Following items describe how the sequence is processed within the modular tool:

1. Impactor selection or definition: if the cascade impactor used is not already present in the list of pre-defined impactors, the user is asked to input the ($d_{p,50}$, s)-values for the N stages. Optionally, the collection efficiency and deposition probabilities can be displayed to check whether the cascade impactor chosen is well defined;
2. Data entry: the user is asked to enter the data (*i.e.* masses, mass concentrations, or any quantifiable parameter) measured for each stage of the cascade impactor. The uncertainty associated to each of the data, notated σ_i, can be added in this window. In this case, the error accepted for each stage (ϵ_i) is taken equal to σ_i, otherwise it can be acquainted later in the inversion window;
3. The histogram corresponding to the aerosol size distribution is displayed;
4. The inversion window appears where inversion parameters (number of consecutive smoothing loops, roughness variation condition, error accepted ϵ_i) are automatically pre-filled with a set

of "universal" values. The user is allowed to modify all of them if necessary;

5. Once realized, the inversion result corresponds to a continuous curve having from 100 to 1000 points and can be directly exported to an Excel Worksheet for further analysis.

When uncertainties (σ_i) have been informed, an additional option consists in determining the experimental error at each point of the inverse curve. Several consecutive inversions are performed, each of them being realized on a random-generated size distribution within each channel confidence interval, leading to statistical variations for each point of the inverse curve.

3. Application to the SIOUTAS personal cascade impactor

3.1. Introduction

This software was originally developed for the case of the SIOUTAS personal cascade impactor (SKC inc, USA). This impactor contains four impaction stages where particles are accelerated in rectangular-shaped nozzles and collected on 0.5 µm-PTFE 25mm filters and a terminal filter consisting in a 2 µm-PTFE 37 mm filter. The SIOUTAS personal impactor has a nominal flow rate of 9 $L.min^{-1}$.

Besides the collection efficiency curves described by [23], the aspiration efficiency was calculated for thin-walled probe and upwards sampling according to Su and Vincent [31]. Terminal filter efficiency is assumed to be 100% whatever particle size. This could be improved by implementing filtration models related to the filter characteristics (filter solid fraction, gas velocity, etc.) as described for example by Raynor *et al.* [32].

We performed mathematical adjustment based on the experimental data from [23] with substrates used without any coating or adhesive material; this led to the stage parameters gathered in Table 1.

Table 1. Stage characteristics of the SIOUTAS personal impactor.

stage	$d_{p,50}$ (µm)	s (-)
4	2.50	2.79
3	1.00	2.51
2	0.50	1.85
1	0.25	1.88

The corresponding deposition probabilities are displayed in Figure 2.

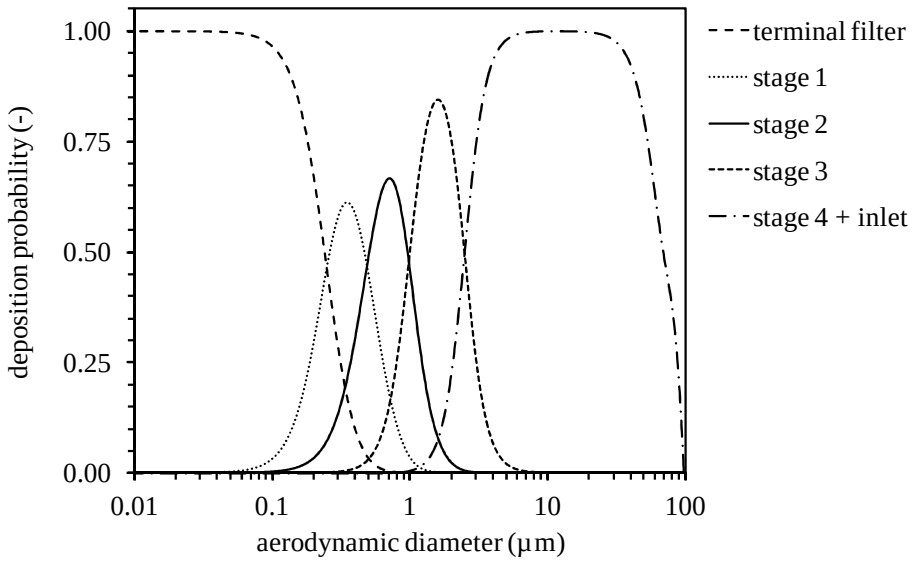

Figure 2. Particle deposition probabilities within the SIOUTAS personal impactor.

It can also be highlighted from Figure 2 that particle overlapping cannot be ignored. Let us take the example of 0.3 µm-particles, attributed to stage 1 according to Table 1. In reality, only 58% of them will deposit on stage 1, while 28% will be found on the terminal filter and 14% collected on stage 2. It is even worth for particles of 1 µm in diameter, presenting 47% deposition probability on stage 2 and 49% on stage 3. As a consequence, it is crucial to take into account the collection efficiency curves when inverting cascade impactors data.

3.2. Theoretical inversions (validation of the calculation procedure)

To validate the inversion method, a series of theoretical data corresponding to the particle mass on each stage was calculated according to the following procedure: (1) definition of the "input" particle size distribution, (2) deposition on the different stages based on collection efficiency curves, and (3) calculation of the quantity of particles collected on each impaction stage. After inversion, the resulting curve ("output") was compared to the original one.

As an example, Figure 3 presents input and output distributions for the case of a bimodal aerosol ($\mathrm{mode}_1 = 0.5\ \mu\mathrm{m}, \sigma_{g,1} = 2, \alpha_1 = 40\%, \mathrm{mode}_2 = 3\ \mu\mathrm{m}, \sigma_{g,2} = 2$), as well as the deposition of particles on the different stages and the corresponding histogram.

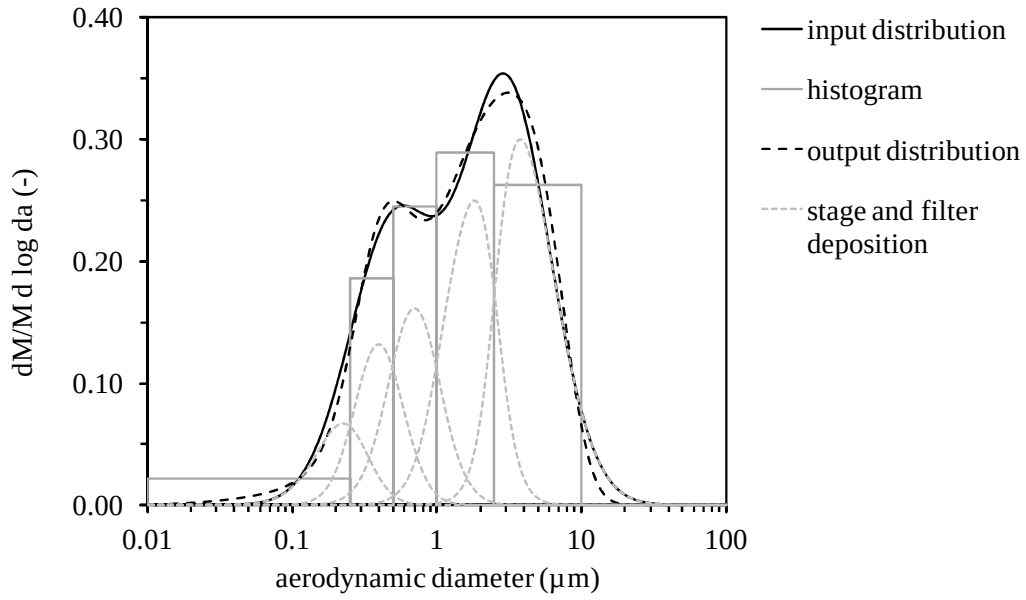

Figure 3. Particle deposition within the SIOUTAS personal impactor for the considered theoretical aerosol, input and output distributions.

Although the histogram (in grey) does not indicate the presence of two populations, the inverse curve resulting from the computation is found to be bimodal and in good agreement with the input size distribution. In such case, it is probable that an adjustment procedure would not bring out the presence of two populations.

For the case corresponding to Figure 3, Fredholm equations are satisfied within $\epsilon_i = 1\ \mu\mathrm{g}$, as shown in Table 2.

Table 2. Comparison of input and output masses (theoretical case).

Stage	terminal	1	2	3	4
Input mass (mg)	0.072	0.129	0.170	0.265	0.364
Output calculated mass (mg)	0.072	0.128	0.171	0.264	0.364

A set of 18 theoretical cases was studied to validate the inversion procedure. Among them, 12 cases correspond to monomodal lognormal aerosols (mode between 0.2 µm and 10 µm, geometric standard deviation between 1.1 and 3) and 6 to bimodal lognormal aerosols. In 65% of the cases, the masses stemming from the inverse curve agreed the initial ones within ± 1 µg, 94% within ± 2 µg and 100% within ± 5 µg, as shown in Figure 4.

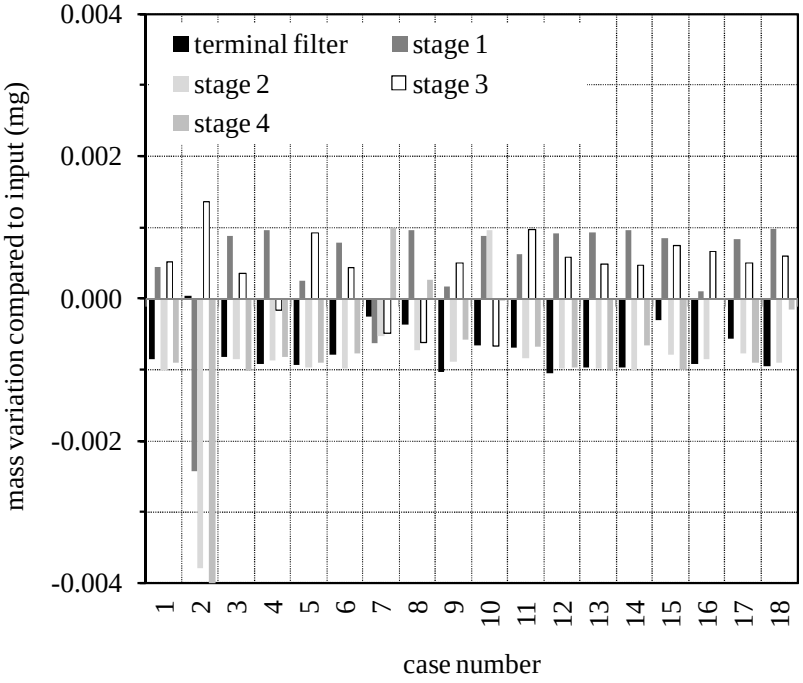

Figure 4. Mass variations between input and calculated from inverse curve for the different stages of the SIOUTAS personal impactor for theoretical cases.

Furthermore, it should be reminded that an inversion problem does not accept a unique solution. Consequently, in addition to the masses per stage, the shape of the curve was examined. In particular, the comparison between input and output distributions was based on observing the concordance of the modal diameter(s), the standard deviation(s) and the height of the curve – without quantified criteria. These observations indicate a good agreement between input and output distributions in most of the cases. Although not universal, it can be concluded that the inversion procedure is valid.

3.3. Example of application of the inversion tool to real measurement data

The first set of data results from a study performed by Witschger *et al.* [33] investigating the potential for exposure from cleanout operations by sandpapering of a reactor producing nanocomposite thin films embedded with silver nanoparticles (~ 8 nm).

Close to the source of sandpapering operation, the total mass concentration was 459 µg.m$^{-3,}$ while the silver mass concentration was 89 µg/m^3, with a bimodal mass size distribution confirmed by electron microscope observations (modal sizes of ~200 nm and 4 µm). Figure 5 displays the mass distribution measured by ICP-MS and the corresponding inverse curve. If the finer mode is in agreement with microscope observations, the coarse one is found around 9 µm in the inverse curve.

Based on ICP-MS elemental composition, the density of the collected particles – mainly containing silver, copper, nickel and iron – was estimated to be 8.5 g.cm^{-3}. The particle dynamic shape factor was taken equal to 1.3. From these parameters and assuming that the particle size stemming from electron microscope pictures is the particle volume equivalent diameter, the corresponding aerodynamic diameter was found to be 10 µm, which is in agreement with the mode observed in the inverse curve.

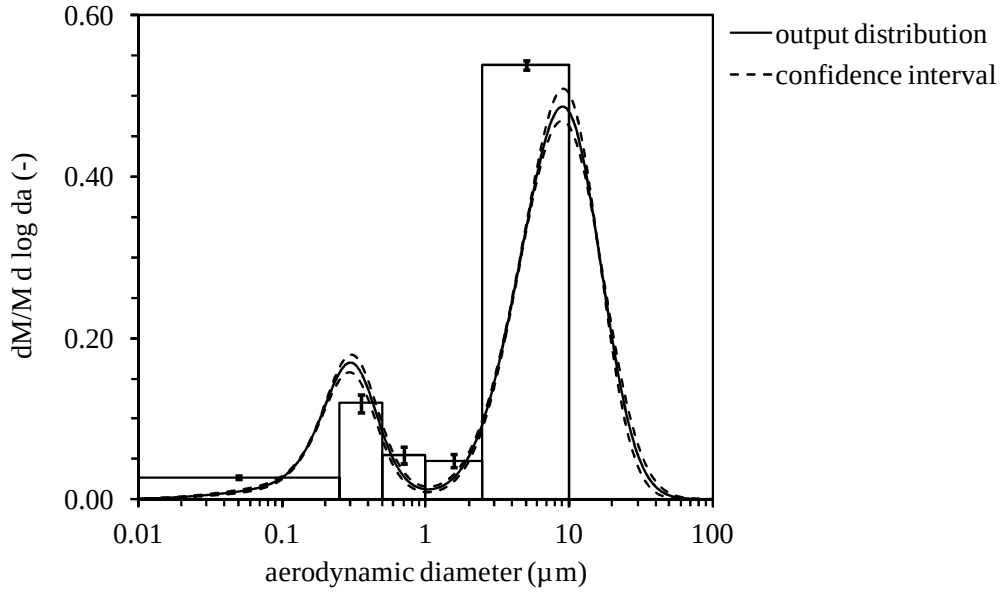

Figure 5. Output distribution and associated confidence interval from airborne silver particles emitted by sandpapering operation – data from [33].

Moreover, the inverted data from total mass collected on each stage (data not shown) was used to calculate the respirable fraction of the aerosol according to CEN [2]. This fraction was found to be 42% of the total mass concentration when the calculation is applied to the inverted data, and 55% when performed on the raw data.

A second set of data was provided by Simon *et al.* [34] in the frame of characterizing airborne actinomycetes (*Thermoactinomyces vulgaris*) produced by means of a liquid sparging generator described in [35]. In this case, the quantities measured on each of the impaction stages correspond to the amount of cultivable bacteria (notated C_B), as shown in Figure 6.

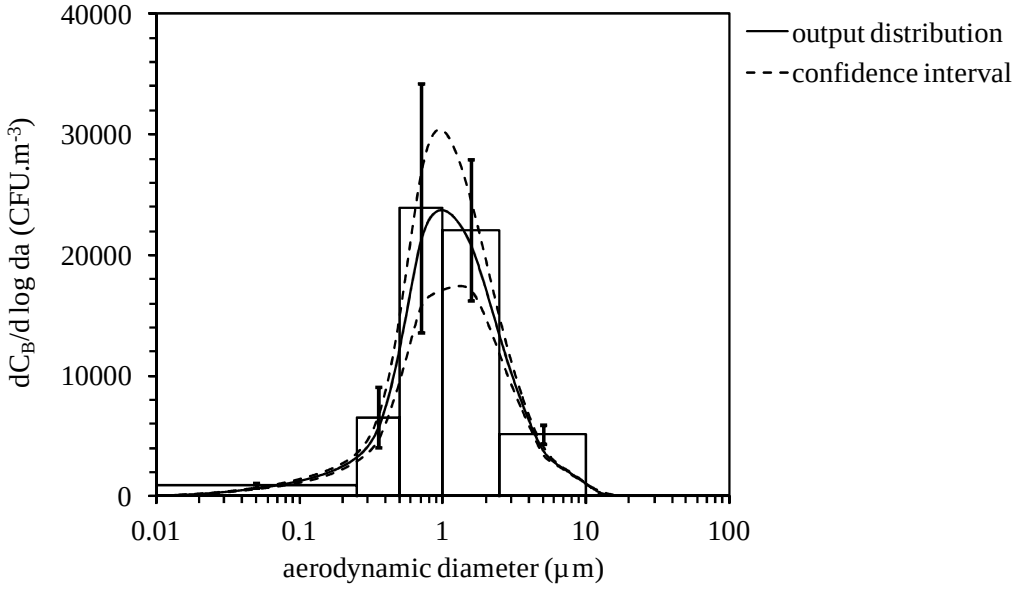

Figure 6. Output distribution and associated confidence interval from cultivable bacteria resulting from the generation of *T. vulgaris* – data from Simon *et al.* [34].

Although Reponen *et al.* [36, 37] measured airborne spores' aerodynamic diameters of 0.57-0.60 µm for *Thermoactinomyces vulgaris*, the inverse curve shows a widespread distribution with a modal size near 1 µm. This indicates the presence of cultivable species other than isolated spores in each of the impaction stages, which can be attributed to mycelium, fragments and agglomerates of various sizes.

4. Discussion and conclusions

A modular tool was developed to inverse data from cascade impactors based on a precise description of the collection efficiency curves. A series of theoretical tests has led to satisfying agreement between input and output distributions for the case of the SIOUTAS personal cascade impactor.

Before being applied to any other widespread cascade impactor (e.g. DLPI — Differential Low Pressure Impactor —, MARPLE, etc.), the inversion software has to be theoretically tested by means of a similar set of data to ensure relevance of the results.

This program is perfectible, and further developments are still needed. Among them:

- diffusion losses are not taken into account in the actual version of the software;
- the aspiration efficiency is only valid for the case of the SIOUTAS impactor;
- calculation of lung-deposited or conventional fractions could be automated;
- terminal filter efficiency has to be improved by the implementation of a filtration model;
- for the cases where extreme stages reveal the highest amount, fictive stages can be required to avoid divergence of the computation. This feature already exists in the program but a series of specific test cases has to be proceeded for validation.

Acknowledgments

Authors would like to thank Noël Castignolles from ESSTIN Services for developing the code and Xavier Simon from INRS for providing experimental data of Figure 6.

References

[1] Maynard A. D., Aitken R. J., Butz T., Colvin V., Donaldson K., Oberdörster G., Philbert M. A., Ryan J., Seaton A., Stone V., Tinkle S. S., Tran L., Walker H. J. and Warheit D. 2006. *Nature* **444**: 267-269.

[2] Comité Européen de Normalisation (CEN) 1993. *Workplace Atmospheres: Size Fraction Definitions for Measurement of Airborne Particles in the Workplace*, CEN standard EN 481.

[3] Brouwer D. 2010. *Toxicology* **269**: 120-127.

[4] Kuhlbusch T., Asbach C., Fissan H., Göhler D. and Stintz M. 2011. *Particle and Fiber Toxicology* **8**: 22.

[5] Ramachandran G., Ostraatb M., Evans D. E., Methner M. M., O'Shaughnessy P., D'Arcy J., Geraci C. L., Stevenson E., Maynard A. D. and Rickabaugh K. 2011. *Journal of Occupational and Environmental Hygiene* **8**: 673-685.

[6] Witschger O., LeBihan O., Reynier M., Durand C., Marchetto A., Zimmermann E. and Charpentier D. 2012. *Hygiène et Sécurité au Travail* **226**: 41-55.

[7] ISO 2008. *Nanotechnologies — Health and safety practices in occupational settings relevant to nanotechnologies*, ISO/TR 12885.

[8] Dong Y., Hays M. D., Smith N. D. and Kinsey J. S. 2004. *Journal of Aerosol Science* **35**: 1497-1512.

[9] ICRP 1994. *Publication 66. Human respiratory tract model for radiological protection*, Oxford: Pergamon.

[10] ISO 2012. *Air quality — Sampling conventions for airborne particle deposition in the human respiratory system*, (EN) ISO 13138.

[11] Heitbrink W. A., Evans D. E., Ku B. K., Maynard A. D., Slavin T. and Peters T. 2009. *Journal of Occupational and Environmental Hygiene* **6**: 19-31.

[12] Maynard A. D. and Aitken R. J. 2007. *Nanotoxicology* **1**: 26.

[13] Marple V. A. and Olson B. A. 2011. *Sampling and measurement using inertial, gravitational, centrifugal, and thermal techniques*, in: Kulkarni P., Baron P. A. and Willeke K., *Aerosol measurement. Principles, techniques and applications*, Third edition, John Wiley & Sons, Inc., 129-151.
[14] Hinds W. C. 1999. *Aerosol Technology. Properties, behavior, and measurement of airborne particles*, Second edition, John Wiley & Sons, Inc., 483 p.
[15] Arffman A., Marjamäki M. and Keskinen J. 2011. *Journal of Aerosol Science* **42**: 329-340.
[16] Demokritou P., Lee S. J., Ferguson S. T. and Koutrakis P. 2004. *Journal of Aerosol Science* **35**: 281-299.
[17] Hillamo R., Mäkelä T., Schwarz J. and Smolik J. 1999. *Journal of Aerosol Science* **33**: S901-S902.
[18] Hillamo R. E. and Kauppinen E. I. 1991. *Aerosol Science and Technology* **14**: 33-47.
[19] Keskinen J., Pietarinen K. and Lehtimäki M. 1992. *Journal of Aerosol Science* **23**: 353-360.
[20] Kwon S. B., Lim K. S., Jung J. S., Bae G. N. and Lee K. W. 2003. *Journal of Aerosol Science* **34**: 289-300.
[21] Marjamäki M., Keskinen J., Chen D. R. and Pui D. Y. H. 2000. *Journal of Aerosol Science* **31**: 249-261.
[22] Marjamäki M., Lemmetty M. and Keskinen J. 2005. *Aerosol Science and Technology* **39**: 575-582.
[23] Misra C., Singh M., Shen S., Sioutas C. and Hall P. M. 2002. *Journal of Aerosol Science* **33**: 1027-1047.
[24] Rubow K. L., Marple V. A., Olin J. and McCawley M. A. 1987. *American Industrial Hygiene Association Journal* **48**: 532-538.
[25] Vaughan N. P. 1989. *Journal of Aerosol Science* **20**: 67-90.
[26] Virtanen A., Marjamäki M., Ristimäki J. and Keskinen J. 2001. *Journal of Aerosol Science* **32**: 389-401.
[27] Twomey S. 1975. *Journal of Computational Physics* **18**: 188-200.
[28] Chahine M. T. 1968. *Journal of the Optical Society of America* **12**: 1634-1637.
[29] Markowski G. R. 1987. *Aerosol Science and Technology* **7**: 127-141.
[30] Winklmayr W., Wang H.-C. and John W. 1990. *Aerosol Science and Technology* **13**: 322-331.
[31] Su W.-C. and Vincent J. H. 2004. *Journal of Aerosol Science* **35**: 1119-1134.
[32] Raynor P. C., Leith D., Lee K. W. and Mukund R. 2011. *Sampling and analysis using filters*, in: Kulkarni P., Baron P. A. and Willeke K., *Aerosol measurement. Principles, techniques and applications*, Third edition, John Wiley & Sons, Inc., 107-128.
[33] Witschger O., Bau S., Bianchi B., Wrobel R. and Matera V. 2013. *Journal of Physics: Conference Series* **This issue**:
[34] Simon X., Betelli L., Koehler V., Coulais C. and Duquenne P. 2013. *Aerosol Science and Technology* **47**: 158-168.
[35] Simon X., Duquenne P., Koehler V., Piernot C., Coulais C. and Faure M. 2011. *Journal of Aerosol Science* **42**: 517-531.
[36] Reponen T., Gazenko S. V., Grinshpun S. A., Willeke K. and Cole E. C. 1998. *Applied and Environmental Microbiology* **64**: 3807-3812.
[37] Reponen T., Grinshpun S. A., Conwell K. L., Wiest J. and Anderson M. 2001. *Grana* **40**: 119-125.